International Journal of Naval Architecture and Ocean Engineering 13 (2021) 758–771

Contents lists available at ScienceDirect

International Journal of Naval Architecture and Ocean Engineering

journal homepage: http://www.journals.elsevier.com/international-journal-of-naval-architecture-and-ocean-engineering/

Robust singular perturbation control for 3D path following of underactuated AUVs

Ming Lei*, Ye Li, Shuo Pang

Science and Technology on Underwater Vehicle Laboratory, Harbin Engineering University, Harbin, China

ARTICLE INFO

Article history:
Received 30 March 2021
Received in revised form
21 June 2021
Accepted 12 August 2021
Available online 2 September 2021

Keywords:
Autonomous underwater vehicle
Path following
Singular perturbations
Control design
Stability analysis

ABSTRACT

This paper presents a novel control scheme for the three-dimensional (3D) path following of underactuated Autonomous Underwater Vehicle (AUVs) subject to unknown internal and external disturbances, in term of the time scale decomposition method. As illustration, two-time scale motions are first artificially forced into the closed-loop control system, by appropriately selecting the control gain of the integrator. Using the singular perturbation theory, the integrator is considered as a fast dynamical control law that designed to shape the space configuration of fast variable. And then the stabilizing controller is designed in the reduced model independently, based on the time scale decomposition method, leading to a relatively simple control law. The stability of the resultant closed-loop system is demonstrated by constructing a composite Lyapunov function. Finally, simulation results are provided to prove the efficacy of the proposed controller for path following of underactuated AUVs under internal and external disturbances.

1. Introduction

AUV plays an important role in marine activities such as ocean sampling, resource exploration and exploitation, and rescue and search, and so on, since it provides a safe, efficient, and economical way without placing human lives at risk. To fulfill these deep oceanic missions, effective motion control is essential. In view of the different application scenarios, several fundamental motion control problems, such as trajectory tracking (Xu et al., 2015; Elmokadem et al., 2016), formation tracking (Qi, 2014; Park, 2015) and path following (Lapierre et al., 2008; Peymani and Fossen, 2015; Peng et al., 2018a, 2018b), are focused. This article considers the path following control of underactuated AUVs that finds many applications in reality, such as oceanographic survey, target carpet searching and pipeline inspection.

In practical cases, there are many challenges in the motion control of an underactuated AUV, such as complex dynamic behavior, parameter variations, model errors and external disturbances caused by sea currents and waves. All these make the motion control of an underactuated AUV attractive to researchers. During the past two decades, a wide range of different nonlinear control techniques have been applied to study this issue and many results are reported. On account of the ability to improve its performance in case of little or no information of the bounds on uncertainties, the adaptive control represents a mainstream method for the motion control of AUVs subject to system uncertainties. In Do et al. (2004), a nonlinear robust adaptive control strategy is developed for path following of underactuated AUVs, based on Lyapunov's direct method, backstepping and parameter projection techniques. In Aguiar and Hespanha (2007), an adaptive switching control scheme is designed for 3D trajectory tracking and path following of underactuated AUVs. In Lapierre and Jouvencel (2008), a hybrid adaptation scheme is proposed to enhance the robustness against the parametric uncertainty. Due to the insensitivity to model uncertainties and unknown disturbances, the Sliding Mode Control (SMC) becomes another mainstream method for the control of AUVs. In Elmokadem et al. (2016), a sliding mode control scheme is proposed for the lateral trajectory tracking of an underactuated AUV. In Xu et al. (2015), a trajectory tracking controller is obtained by the combining the backstepping technique and adaptive dynamical SMC. To eliminate the main drawback associated with the SMC, known as the chattering effect due to the discontinuous control signal, in Salgado-Jimenez et al. (2004) and Joe et al. (2014), two different higher order sliding mode control schemes are introduced.

* Corresponding author.
E-mail address: shandian2010@hrbeu.edu.cn (M. Lei).
Peer review under responsibility of The Society of Naval Architects of Korea.

https://doi.org/10.1016/j.ijnaoe.2021.08.003

Since Fuzzy Logic Systems (FLS) and Neural Networks (NN) are capable to approximate nonlinearities, as a result, provide improved robustness properties under model uncertainties and unknown disturbances, they have been widely used in the control system design. In Zhang et al. (2009), an adaptive output feedback controller is designed for the 3D trajectory tracking of AUVs, based on Dynamic Recurrent Fuzzy Neural Network (DRFNN). In Xiang et al. (2017), a robust fuzzy control law is proposed for 3D path following of AUVs. In Peng et al. (2019), anti-disturbance constrained control of AUVs subject to uncertainties and constraints is developed, using NN approach and observer-based technique. As illustration, all these nonlinear control techniques mentioned above have the advantages on addressing the technical challenges of model uncertainties and unknown external disturbances. However, they usually yield relatively complicated controllers which may be prohibitive in the real world.

As a simple but effective tool for dealing with the unknown disturbances of complex system, the observer-based control technique has also drawn obvious attentions of researchers for the control system design given unknown external and internal disturbances. In Fernandes et al. (2015), a high-gain observer-based output feedback control law is employed for Remotely Operated Vehicles (ROVs), considering the model errors, measurement errors, and unknown external environmental disturbances. In Peng et al. (2018a and 2018b), two controllers with different focuses are developed for path-following of underactuated AUVs based on Extended State Observer (ESO) and NN.

Theory of singular perturbation and time scale represents a mathematical realization of intuitive approach to simplified models obtained via order reduction (Kokotovic et al., 1999; Khalil, 2002). Compared to most classical control methods, the distinct feature of singular perturbation control is that it allows a time scale decomposition of a dynamic system into lower order subsystems with different time scales, in which the control laws can be designed independently and thus being easily obtained, leading to a reduction of control complexity. Such characteristic is deeply appealing to researchers and control engineers. It has been widely applied to the design and analysis of motion control of marine vehicles. In Canudas and Olguin (2000), a robust nonlinear feedback control law is developed for ROVs equipped with a robot manipulator, by utilizing the difference between the two-time operation scale between the vehicle and the manipulator. In Bhatta and Leonard (2008), several Lyapunov-based controllers are proposed for wing-level flight of underwater gliders with different configurations. Following that, Zhang and Tan (2015) design a nonlinear, passivity-based controller and an observer for a gliding robotic fish, based on the existing reduced subsystem as in Bhatta and Leonard (2008). In Ren et al. (2014) and Yi et al. (2016), two distinct two-time scale singular perturbation control laws are employed for Rudder Roll Stabilization (RRS) and path following of marine surface vessels, respectively. Prestero (2001) proposes a simple inner-and-outer loop PD controller for the pitch-depth diving motion of an underactuated AUV, by taking advantages of the time scale separation between the translational dynamics and orientation dynamics. However, no analytical results are provided. With this problem, recently, Lei (2020) provides a singular perturbation analysis for the dive control of underactuated AUVs.

In this paper, a method is presented for the path following control of underactuated AUVs subject to model uncertainties and unknown environmental disturbances. To provide an easy-to-implement controller, we resort to the integral control technique. The controller is divided into two parts: integrator and stabilizing controller. By appropriately selecting the control gain, two-time scale motions are artificially forced into the extended closed-loop control system, thus, the properties of system is analyzed, in term of the theory of singular perturbation and time scale. In that case, the integrator is naturally considered as a fast dynamical control law, which is designed to shape a desired space configuration of fast variable, so as to obtain an ideal reduced model without system uncertainties. The design of stabilizing controller thereby becomes a model-based control problem. To further reduce the control complexity, a forced singular perturbation method is utilized, with a realistic assumption: the translational and angular velocities are much faster than the kinematic tracking errors, at the same time, the path angle tracking errors are faster than the cross-track errors. On the basis of that, the control law is obtained by designing respective control schemes for each subsystem that given by time scale decomposition. And the stability analysis of the reduced model is performed by constructing a composite Lyapunov function. Meanwhile, the mathematical bounds on the control gains are also provided. Finally, its control performance is evaluated through computer simulations. They show that the proposed control scheme is robust in the presence of unknown internal and external disturbances, and a good path following performance is guaranteed.

The remainder of the paper is organized as follows. Section 2 states the problem formulation. Section 3 and Section 4 present the design and analysis of path following controller via singular perturbation technique. Section 5 presents the simulation results to illustrate the control performance. Section 6 concludes this paper.

2. Preliminaries

The kinematic and dynamic models of an underactuated AUV is presented, and a formulation of the 3D path following control problem is stated.

2.1. Model of an underactuated AUV

To study the motion of an underactuated AUV, we first define two reference frames: {I} and {B}. As illustrated in Fig. 1, the inertial frame {I} is defined by an orthonormal triad $\{\boldsymbol{i}_1,\boldsymbol{i}_2,\boldsymbol{i}_3\}$, where $\boldsymbol{i}_1$ and $\boldsymbol{i}_2$ lie along the horizontal plane, perpendicular to gravity. And $\boldsymbol{i}_3$ lies in the direction of the gravity vector and is positive in the downward direction. The origin of body-fixed frame {B} locates at the center of buoyancy (CB), where the $\boldsymbol{b}_1$ points to the fore along the longitudinal axis of an AUV, the $\boldsymbol{b}_2$ points to the starboard of an AUV, and the $\boldsymbol{b}_3$ is determined by the right-hand rule. Following that, we define some symbols as in Table 1.

In the present study, we ignore the dynamics of roll and surge, with assumption of that $\phi = 0$ and the surge velocity u is fixed. This is realistic when the vehicle has an effective forward speed controller and is equipped with independent roll actuators (Rezazadegan et al., 2015). Accordingly, the kinematic model of an AUV can be expressed as

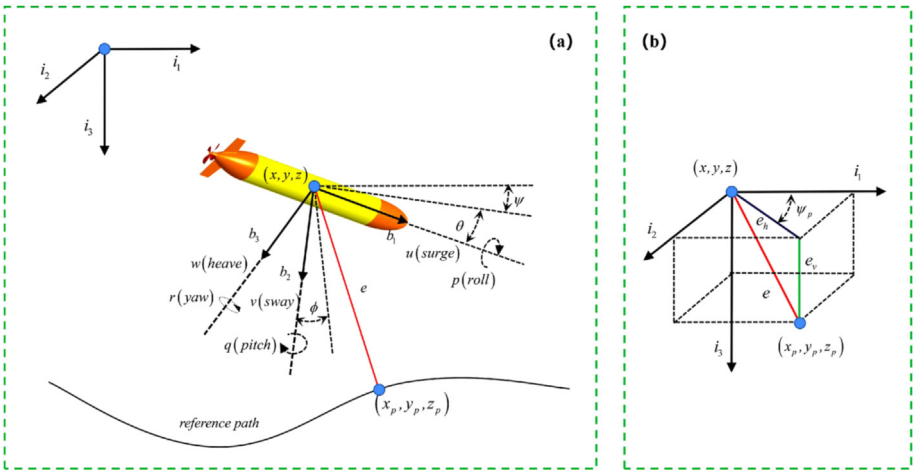

Fig. 1. (a) Vehicle model and reference frames; (b) kinematic path following errors.

Table 1
Definition of symbols.

Symbol	Description
(x,y,z)	vehicle's positions with respect to the frame {I}
(u,v,w)	vehicle's translational velocities (surge, sway and heave, respectively) expressed in the frame {B}
(ϕ,θ,ψ)	vehicle's attitude (the roll, pitch and yaw angles, respectively)
(p,q,r)	vehicle's angular velocities about each of the axis of the frame {B}

$$\begin{cases} \dot{x} = u\cos(\psi)\cos(\theta) - v\sin(\psi) + w\cos(\psi)\sin(\theta) \\ \dot{y} = u\sin(\psi)\cos(\theta) + v\cos(\psi) + w\sin(\psi)\sin(\theta) \\ \dot{z} = -u\sin(\theta) + w\cos(\theta) \\ \dot{\theta} = q \\ \dot{\psi} = r/\cos(\theta) \end{cases} \tag{1}$$

and the simplified kinetic model can be written as

$$\begin{cases} \dot{v} = \dfrac{1}{m_{22}}(-m_{11}ur - d_{22}v) \\ \dot{w} = \dfrac{1}{m_{33}}(m_{11}uq - d_{33}w) \\ \dot{q} = \dfrac{1}{m_{55}}(-mgz_g\sin(\theta) + (m_{33}-m_{11})uw - d_{55}q + \tau_q + d_q) \\ \dot{r} = \dfrac{1}{m_{66}}((m_{11}-m_{22})uv - d_{66}r + \tau_r + d_r) \end{cases} \tag{2}$$

where, $m_{11} = m - X_{\dot{u}}$, $m_{22} = m - Y_{\dot{v}}$, $m_{33} = m - Z_{\dot{w}}$, $m_{55} = I_{yy} - M_{\dot{q}}$, $m_{66} = I_{zz} - N_{\dot{r}}$, $d_{22} = -Y_v - Y_{v|v|}$, $d_{33} = -Z_w - Z_{w|w|}$, $d_{55} = -M_q - M_{q|q|}$, $d_{66} = -N_r - N_{r|r|}$. Here, m and $I_{(\cdot)}$ represent vehicle's mass and moment of inertia. $X_{(\cdot)}$, $Y_{(\cdot)}$, $Z_{(\cdot)}$, $M_{(\cdot)}$ and $N_{(\cdot)}$ denote vehicle's hydrodynamic parameters, including the damping and added mass in surge, sway, heave, pitch and heading, respectively. d_q and d_r account for the unknown internal and external disturbances.

2.2. Kinematic path following error dynamics

In this subsection, the kinematic error dynamics for path following is derived. The 3D case is divided into two parts: horizontal-plane path following and depth tracking, contributing to providing a simpler approach. As illustrated in Fig. 1(b), e_h represents the cross-track error in the horizontal plane, while e_v represents the depth tracking error. Let e denote the total cross-track error, it is clear to see that $\vec{e} = \vec{e_h} + \vec{e_v}$, $\|e\| \le \|e_h\| + \|e_v\|$, and $e \to 0$ in case of $e_h \to 0$ and $e_v \to 0$. Therefore, our goal is converted into stabilize e_v and e_h to zero, independently.

2.2.1. Tracking error dynamics in the diving direction

The depth error is

$$e_v = z - z_p \tag{3}$$

The time-derivative of e_v gives

$$\begin{aligned} \dot{e}_v &= -u\sin(\theta) + w\cos(\theta) - \dot{z}_p = -U_0\sin(\theta - \alpha) - \dot{z}_p \\ &= -U_1\sin(\theta_e - \alpha) \end{aligned} \tag{4}$$

where $U_0 = \sqrt{u^2 + w^2} > 0$, $U_1 = \sqrt{u^2 + w^2 + [\dot{z}_p/\cos(\theta - \alpha)]^2} > 0$, $\alpha = \text{atan2}(w, u)$. θ_p is recognized as the designed desired pitch

angle, in order to track the depth along the reference path, and given by

$$\theta_p = \arctan\left(\frac{-\dot{z}_p}{U_0\cos(\theta-\alpha)}\right) \tag{5}$$

In this case, $\theta_e = \theta - \theta_p$ represents the pitch angle tracking error. And the pitching error dynamics is

$$\dot{\theta}_e = q - q_p \tag{6}$$

Here, $q_p = \dot{\theta}_p$ is a desired angular velocity for the point (x_p, y_p, z_p) along the reference path.

2.2.2. Path following error dynamics in the horizontal plane

Referring to (Lekkas and Fossen, 2013), the cross-track e_h can be taken as

$$e_h = -(x-x_p)\sin(\psi_p) + \left(y-y_p\right)\cos(\psi_p) \tag{7}$$

where $\psi_p = \text{atan2}(\dot{y}_p, \dot{x}_p), (\dot{x}_p \neq 0)$ is the path-tangential angle for point (x_p, y_p) along the path projected on the horizontal plane. The derivative $\dot{e}_h$ is

$$\begin{aligned}\dot{e}_h &= -\dot{x}\sin(\psi_p) + \dot{y}\cos(\psi_p)\\ &= -[u\cos(\psi)\cos(\theta) - v\sin(\psi) + w\cos(\psi)\sin(\theta)]\sin(\psi_p)\\ &\quad +[u\sin(\psi)\cos(\theta) + v\cos(\psi) + w\sin(\psi)\sin(\theta)]\cos(\psi_p)\\ &= \sqrt{u^2+w^2}\cos(\theta-\alpha)\sin(\psi_e) + v\cos(\psi_e)\\ &= U_2\sin(\psi_e+\beta_n)\end{aligned} \tag{8}$$

Here $U_2 = \sqrt{U_0^2\cos^2(\theta-\alpha)+v^2} > 0$ and $\beta_n = \text{atan2}(v, U_0\cos(\theta-\alpha))$ respectively denote the nominal moving velocity and sideslip angle with respect to the horizontal path following motion. $\psi_e = \psi - \psi_p$ is the yaw angle tracking error. Following that, the yawing error dynamics is

$$\dot{\psi}_e = r/\cos(\theta) - r_p \tag{9}$$

where, $r_p = \dot{\psi}_p$ are considered as the desired angular velocities for the point (x_p, y_p) along the reference path projected on the horizontal plane.

2.3. Control system and control objective

As illustration above, the mathematical model for 6-DOFs path following control of an underactuated AUV is written as

$$\begin{cases}\dot{e}_v = -U_1\sin(\theta_e-\alpha)\\ \dot{e}_h = U_2\sin(\psi_e+\beta_n)\\ \dot{\theta}_e = q - q_p\\ \dot{\psi}_e = \dfrac{1}{\cos(\theta)}r - r_p\\ \dot{v} = \dfrac{1}{m_{22}}(-m_{11}ur - d_{22}v)\\ \dot{w} = \dfrac{1}{m_{33}}(m_{11}uq - d_{33}w)\\ \dot{q} = \dfrac{1}{m_{55}}(-mgz_g\sin(\theta) + (m_{33}-m_{11})uw - d_{55}q + \tau_q + d_q)\\ \dot{r} = \dfrac{1}{m_{66}}((m_{11}-m_{22})uv - d_{66}r + \tau_r + d_r)\end{cases} \tag{10}$$

The control goal herein is to design a control law for τ_q and τ_r in (10) to stabilize the tracking errors e_v and e_h, so as to force an underactuated AUV to follow a prescribed path. It assumes that all the states are measurable, except for the acceleration information.

3. Integral controller

In this section, we first consider the problem of control system design given unknown disturbances. To this end, an integral control law is discussed. The overall design and analysis is as follows.

3.1. Control design

In order to reach the objective of developing a nonlinear controller that should be easy to implement in reality, a simple integral control scheme is considered.

$$\begin{cases}\tau_q = \tau_{q1} + \tau_{q2}\\ \tau_r = \tau_{r1} + \tau_{r2}\\ \lambda_q\dot{\tau}_{q2} = \dfrac{1}{m_{55}}(-mgz_g\sin(\theta) + (m_{33}-m_{11})uw - d_{55}q + \tau_{q1}) - \dot{q}\\ \lambda_r\dot{\tau}_{r2} = \dfrac{1}{m_{66}}((m_{11}-m_{22})uv - d_{66}r + \tau_{r1}) - \dot{r}\end{cases} \tag{11}$$

where, λ_q and λ_r are small positive parameters and satisfies $0 < \lambda_{(\cdot)} \ll 1$. Note that the design parameters λ_q and $\lambda_r$should be chosen properly according to the physical limitations on the vehicle's control inputs. τ_{q1} and τ_{r1} are stabilizing controller, while τ_{q2} and τ_{r2} are integral controller that can be written as

$$\begin{cases}\tau_{q2} = \dfrac{1}{\lambda_q}\left\{\dfrac{1}{m_{55}}\left[-mgz_g\sin(\theta) + (m_{33}-m_{11})uw - d_{55}q + \tau_{q1}\right]dt - q(t)\Big|_{t_0}^{t_n}\right\}\\ \tau_{r2} = \dfrac{1}{\lambda_r}\left\{\displaystyle\int_{t_0}^{t_n}\dfrac{1}{m_{66}}[(m_{11}-m_{22})uv - d_{66}r + \tau_{r1}]dt - r(t)\Big|_{t_0}^{t_n}\right\}\end{cases} \tag{12}$$

and thereby independent of vehicle's acceleration information. It is therefore achievable in reality.

Using (11), the mathematical model for path following control is put into an extended-state model as follow.

$$\begin{cases} \dot{e}_v = -U_1 \sin(\theta_e - \alpha) \\ \dot{e}_h = U_2 \sin(\psi_e + \beta_n) \\ \dot{\theta}_e = q - q_p \\ \dot{\psi}_e = \dfrac{1}{\cos(\theta)} r - r_p \\ \dot{v} = \dfrac{1}{m_{22}}(-m_{11} ur - d_{22} v) \\ \dot{w} = \dfrac{1}{m_{33}}(m_{11} uq - d_{33} w) \\ \dot{q} = \dfrac{1}{m_{55}}((m_{33} - m_{11}) uw - d_{55} q + mgz_g \sin\theta + \tau_q + d_q) \\ \dot{r} = \dfrac{1}{m_{66}}((m_{11} - m_{22}) uv - d_{66} r + \tau_r + d_r) \\ \lambda_q \dot{\tau}_{q2} = \dfrac{1}{m_{55}}((m_{33} - m_{11}) uw - d_{55} q + mgz_g \sin(\theta) + \tau_{q1}) - \dot{q} \\ \lambda_r \dot{\tau}_{r2} = \dfrac{1}{m_{66}}((m_{11} - m_{22}) uv - d_{66} r + \tau_{r1}) - \dot{r} \end{cases} \tag{13}$$

where, τ_{q2} and τ_{r2} denote extended states. It is clear to see that the small parameters λ_q and λ_r force three (possibly) different time scales into the above system (13): the slow time scale t, and three fast time scales t/λ_q and t/λ_r. Following the method as in Bhatta and Leonard (2008), we simply consider one fast subsystem that contains all those three fast time scales, by defining a unified fast time scale t/λ, where $\lambda = \max\{\lambda_q, \lambda_r\}$. In that case, e_v, e_h, ψ_e, θ_e, v, w, q and r represent slow variable, while τ_{q2} and τ_{r2} represent fast variable. Prior to the time scale decomposition of system (13), we define two operators ^ and ~, which yield the quasi-steady-state and the boundary layer correction of a state variable, respectively. For more detail about these definitions, one might refer to Kokotovic et al. (1999).

Considering the fast time scale defined by $t_c = t/\lambda$, system (13) is decomposed into two subsystems of lower order, where the fast model is

$$\begin{cases} \dfrac{d\tilde{\tau}_{q2}}{dt_c} = \dfrac{\lambda}{\lambda_q}\left[\dfrac{1}{m_{55}}(-mgz_g \sin(\theta) + (m_{33} - m_{11}) uw - d_{55} q + \tau_{q1}) - \dot{q}\right] = -\dfrac{\lambda}{\lambda_q}\dfrac{1}{m_{55}}\tilde{\tau}_{q2} \\ \dfrac{d\tilde{\tau}_{r2}}{dt_c} = \dfrac{\lambda}{\lambda_r}\left[\dfrac{1}{m_{66}}((m_{11} - m_{22}) uv - d_{66} r + \tau_{r1}) - \dot{r}\right] = -\dfrac{\lambda}{\lambda_r}\dfrac{1}{m_{66}}\tilde{\tau}_{r2} \end{cases} \tag{14}$$

and slow model is

$$\begin{cases} \dot{e}_v = -U_1 \sin(\theta_e - \alpha) \\ \dot{e}_h = U_2 \sin(\psi_e + \beta_n) \\ \dot{\theta}_e = q - q_p \\ \dot{\psi}_e = \dfrac{1}{\cos(\theta)} r - r_p \\ \dot{v} = \dfrac{1}{m_{22}}(-m_{11} ur - d_{22} v) \\ \dot{w} = \dfrac{1}{m_{33}}(m_{11} uq - d_{33} w) \\ \dot{q} = \dfrac{1}{m_{55}}(-mgz_g \sin\theta + (m_{33} - m_{11}) uw - d_{55} q + \tau_{q1}) \\ \dot{r} = \dfrac{1}{m_{66}}((m_{11} - m_{22}) uv - d_{66} r + \tau_{r1}) \end{cases} \tag{15}$$

Here, the quasi-steady-state equilibrium of fast model satisfies the following degenerate equation

$$\begin{cases} 0 = \dfrac{1}{m_{55}}(-mgz_g \sin(\theta) + (m_{33} - m_{11}) uw - d_{55} q + \tau_{q1}) - \dot{q} \\ 0 = \dfrac{1}{m_{66}}((m_{11} - m_{22}) uv - d_{66} r + \tau_{r1}) - \dot{r} \end{cases} \tag{16}$$

thus, given by

$$\begin{cases} \hat{\tau}_{q2} = -d_q \\ \hat{\tau}_{r2} = -d_r \end{cases} \tag{17}$$

Obviously, the space configuration of the fast model is defined only by the unknown internal and external disturbances. It reveals that the integrator can be considered as an ESO which is designed to estimate the required compensation for the unknown disturbances. Also note, τ_{q1} and τ_{r1} can be designed in the reduced model (15) independently.

Remark 1. A distinctive feature of the discussed control scheme is that it allows for an application of the theory of singular perturbation and time scale, providing a deep insight into the properties of closed-loop system (13). Specifically, the integrator is considered as a fast dynamical control law which is designed to shape the desired space configuration of fast variable, so as to obtain an ideal reduced model (15). And then the problem of

control system design given unknown disturbances is reduced to a problem of model-based control.

3.2. Stability analysis

According to Saberi and Khalil (1984), Kokotovic et al. (1999) and Khalil (2002), once the dynamic system is decomposed into two subsystems of lower order, the Lyapunov function candidate for full system can be obtained by constructing a weight sum of the Lyapunov function candidates of two subsystems. On the basis of that, we observe if the asymptotic stability of fast model (14) and slow model (15) is guaranteed, there must be a composite Lyapunov function for proving the asymptotic stability of full order system (13), due to the fact that the design parameters λ_q and λ_r can be sufficiently small. To our knowledge, it is an easy task to prove the asymptotic stability of fast model (14). The Proof is omitted for the sake of brevity. The asymptotic stability analysis for slow model (15) will be detailed in Section 4.

4. Stabilizing controller

In this section, a control law for τ_{q1} and τ_{r1} is designed to stabilize the dynamic model (15), assuming the fast variable has reached its quasi-steady-state and evolve on its own manifold. For simplicity, τ_{q1} and τ_{r1} are chosen as

$$\begin{cases} \tau_{q1} = \overline{\tau}_q + mgz_g \sin(\theta) - (m_{33} - m_{11})uw \\ \tau_{r1} = \overline{\tau}_r - (m_{11} - m_{22})uv \end{cases} \tag{18}$$

It results in

$$\begin{cases} \dot{e}_v = -U_1 \sin(\theta_e - \alpha) \\ \dot{e}_h = U_2 \sin(\psi_e + \beta_n) \\ \dot{\theta}_e = q - q_p \\ \dot{\psi}_e = \dfrac{1}{\cos(\theta)} r - r_p \\ \dot{v} = \dfrac{1}{m_{22}}(- m_{11}ur - d_{22}v) \\ \dot{w} = \dfrac{1}{m_{33}}(m_{11}uq - d_{33}w) \\ \dot{q} = \dfrac{1}{m_{55}}(- d_{55}q + \overline{\tau}_q) \\ \dot{r} = \dfrac{1}{m_{66}}(- d_{66}r + \overline{\tau}_r) \end{cases} \tag{19}$$

followed by the objective to design a control law for $\overline{\tau}_q$ and $\overline{\tau}_r$ to stabilize system (19).

In view of the complexity of model (19), it is still a challenging task for control system design. To reduce the control complexity, the theory of singular perturbation and time scale is used. However, modeling a physical system in the singularly perturbed form may not be easy, due to the fact that it is not always clear how to identify the small singularly perturbed parameters. Following the approach as in Shinar (1983) and Sheu et al. (1991), in this section, a forced singular perturbation model is obtained, by artificial insertion of the singularly perturbed parameters. On an initial inspection of model (19), a three-time scale model is more suitable (see Fig. 2). Specifically, we select r, q, w and v as fast variables; ψ_e and θ_e as slow variables; e_v and e_h as ultra-slow variable. Accordingly, in term of the singular perturbation technique, $\overline{\tau}_q$ and $\overline{\tau}_r$ can be expressed as following form:

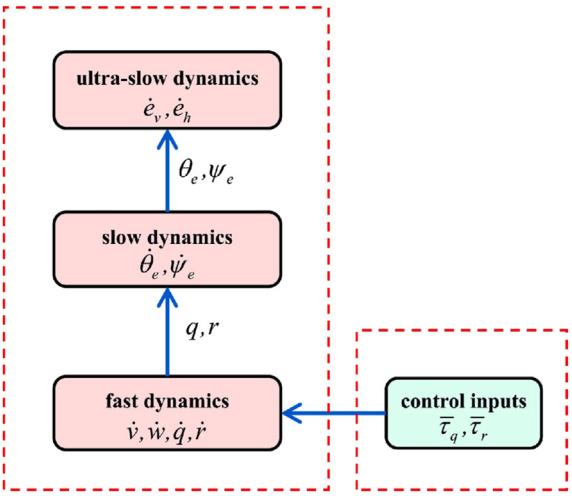

Fig. 2. Block diagram of the AUV dynamics for path-following motion.

$$\overline{\tau}_q = \overline{\tau}_q^{f1} + \overline{\tau}_q^{f2} + \overline{\tau}_q^{s2} \tag{20}$$

$$\overline{\tau}_r = \overline{\tau}_r^{f1} + \overline{\tau}_r^{f2} + \overline{\tau}_r^{s2} \tag{21}$$

where, the superscripts $f1, f2, s2$ denote the control laws for *Layer-1* fast subsystem, *Layer-2* fast subsystem and *Layer-2* slow subsystem, respectively. For more detail about these subsystems, please refer to the following time scale decomposition in section 4.1.

Recalling the time scale separation mentioned above, and using Eqs. (20) and (21), the dynamic model (19) is put into

$$\begin{cases} \dot{e}_v = -U_1 \sin(\theta_e - \alpha) \\ \dot{e}_h = U_2 \sin(\psi_e + \beta_n) \\ \varepsilon_1 \dot{\theta}_e = \mu_1 (q - q_p) \\ \varepsilon_1 \dot{\psi}_e = \mu_1 \left(\dfrac{1}{\cos(\theta)} r - r_p \right) \\ \varepsilon_2 \varepsilon_1 \dot{v} = \mu_2 \dfrac{1}{m_{22}}(- m_{11}ur - d_{22}v) \\ \varepsilon_2 \varepsilon_1 \dot{w} = \mu_2 \dfrac{1}{m_{33}}(m_{11}uq - d_{33}w) \\ \varepsilon_2 \varepsilon_1 \dot{q} = \mu_2 \dfrac{1}{m_{55}} \left(- d_{55}q + \overline{\tau}_q^{f1} + \overline{\tau}_q^{f2} + \overline{\tau}_q^{s2} \right) \\ \varepsilon_2 \varepsilon_1 \dot{r} = \mu_2 \dfrac{1}{m_{66}} \left(- d_{66}r + \overline{\tau}_r^{f1} + \overline{\tau}_r^{f2} + \overline{\tau}_r^{s2} \right) \end{cases} \tag{22}$$

Here, $\varepsilon_{i=1,2}$ are artificial singularly perturbed parameters. $\mu_1 = \varepsilon_1$ and $\mu_2 = \varepsilon_1 \varepsilon_2$.

4.1. Time scale decomposition

This subsection presents the time scale decomposition of system (22). For convenience, we rewrite the three-time scale singularly perturbed system (22) in a compact form as follows:

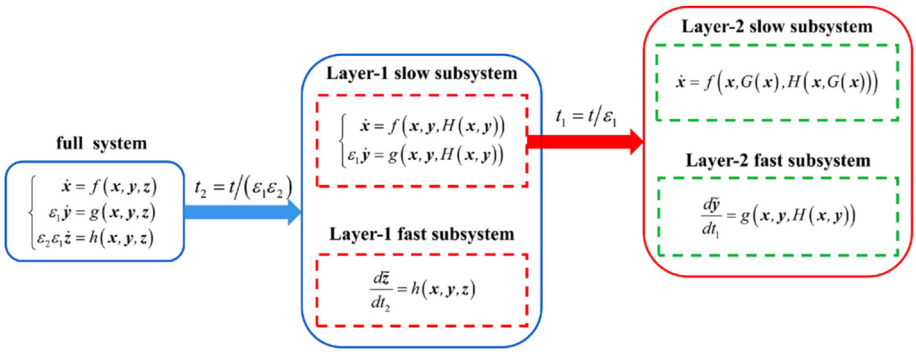

Fig. 3. Three-time scale singular perturbation reduction.

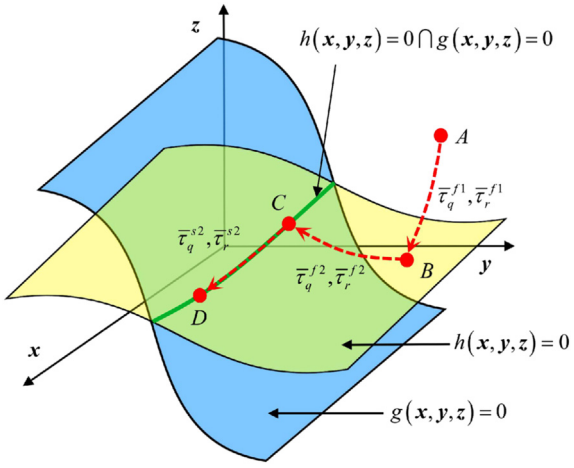

Fig. 4. Control strategy for a three-time scale singularly perturbed system. A is an initial state, B is a state lying on the manifold $0=h(\boldsymbol{x},\boldsymbol{y},\boldsymbol{z})$, C is a state lying on the manifold $0=g(\boldsymbol{x},\boldsymbol{y},\boldsymbol{z})$, D is the desired origin of full system. In a geometric view, the closed-loop system (25) are expected to converge to the desired origin along the designed flow $A\rightarrow B\rightarrow C\rightarrow D$ with control inputs $\bar{\tau}_q^{f1}$, $\bar{\tau}_q^{f2}$, $\bar{\tau}_q^{s2}$, $\bar{\tau}_r^{f1}$, $\bar{\tau}_r^{f2}$ and $\bar{\tau}_r^{s2}$.

$$\begin{cases}\dot{\boldsymbol{x}}=f(\boldsymbol{x},\boldsymbol{y},\boldsymbol{z})\\ \varepsilon_1\dot{\boldsymbol{y}}=g(\boldsymbol{x},\boldsymbol{y},\boldsymbol{z})\\ \varepsilon_2\varepsilon_1\dot{\boldsymbol{z}}=h(\boldsymbol{x},\boldsymbol{y},\boldsymbol{z})\end{cases}\tag{23}$$

Here, $\boldsymbol{x}=(e_v;e_h)$, $\boldsymbol{y}=(\theta_e;\psi_e)$ and $\boldsymbol{z}=(v;w;q;r)$ denote ultra-slow, slow and fast state variables of the three-time scale singularly perturbed system (22), respectively. $f(\cdot)$, $g(\cdot)$ and $h(\cdot)$ are continuously differentiable functions of state variables $\boldsymbol{x}$, $\boldsymbol{y}$ and $\boldsymbol{z}$.

Fig. 3 has provided an intuitive description of singular perturbation reduction. It is clear to see that the generic three-time scale system (23) can be sequentially decomposed into two distinct two-time scale models. The first two-time scale model, that is, *Layer-1*, is obtained by considering the stretched time scale $t_2=t_1/\varepsilon_2\triangleq t/(\varepsilon_1\varepsilon_2)$, where the *Layer-1* fast subsystem, is defined by

$$\frac{d\tilde{\boldsymbol{z}}}{dt_2}=h(\boldsymbol{x},\boldsymbol{y},\tilde{\boldsymbol{z}}+H(\boldsymbol{x},\boldsymbol{y}))\tag{24}$$

and the *Layer-1* slow subsystem, is defined by.

$$\begin{cases}\dot{\boldsymbol{x}}=f(\boldsymbol{x},\boldsymbol{y},H(\boldsymbol{x},\boldsymbol{y}))\\ \varepsilon_1\dot{\boldsymbol{y}}=g(\boldsymbol{x},\boldsymbol{y},H(\boldsymbol{x},\boldsymbol{y}))\end{cases}\tag{25}$$

Note that, $\boldsymbol{x}$ and $\boldsymbol{y}$ are treated as frozen variables during the fast transient (24). $H(\boldsymbol{x},\boldsymbol{y})$ represents the quasi-steady-state of $\boldsymbol{z}$, given by setting $\varepsilon_2=0$, that is, $0=h(\boldsymbol{x},\boldsymbol{y},\boldsymbol{z})\rightarrow\hat{\boldsymbol{z}}=H(\boldsymbol{x},\boldsymbol{y})$. Similarly, the reduced order *Layer-1* slow subsystem (25) can be treated again like a two-time scale singular perturbation problem by considering the stretched time scale $t_1=t/\varepsilon_1$, where the boundary-layer subsystem, denoted by the *Layer-2* fast subsystem, is defined by

$$\frac{d\tilde{\boldsymbol{y}}}{dt_1}=g(\boldsymbol{x},\tilde{\boldsymbol{y}}+G(\boldsymbol{x}),H(\boldsymbol{x},\tilde{\boldsymbol{y}}+G(\boldsymbol{x})))\tag{26}$$

and where the reduced subsystem, denoted by the *Layer-2* slow subsystem, is defined by

$$\dot{\boldsymbol{x}}=f(\boldsymbol{x},G(\boldsymbol{x}),H(\boldsymbol{x},G(\boldsymbol{x})))\tag{27}$$

Also note, $\boldsymbol{x}$ is treated as a frozen variable during the fast transient (26). $G(\boldsymbol{x})$ denotes the quasi-steady-state of $\boldsymbol{y}$, obtained by setting $\varepsilon_1=0$, that is, $0=g(\boldsymbol{x},\boldsymbol{y},H(\boldsymbol{x},\boldsymbol{y}))\rightarrow\hat{\boldsymbol{y}}=G(\boldsymbol{x})$, with assumption of that $\boldsymbol{z}$ has reached its quasi-steady-state and evolve on its own manifold.

4.2. Control design

The previous subsection has provided an intuitive description of time scale decomposition of system (23). In this subsection, the control laws will be designed in each subsystem separately. An intuitive description of control strategy for the three-time scale singularly perturbed system can be seen in Fig. 4.

4.2.1. Control law for the Layer-2 slow subsystem

Proposition 1: The *Layer-2* slow subsystem (27) will be asymptotically stable by selecting a virtual feedback control law

$$\begin{cases}\hat{\theta}_e=k_1e_v+\alpha\\ \hat{\psi}_e=-k_2e_h-\beta_n\end{cases}\tag{28}$$

Here, $k_1>0$, $k_2>0$.

Proof. Using (28), the *Layer-2* slow subsystem (27) is put into

$$\begin{cases}\dot{e}_v=-U_1\sin(k_1e_v)\\ \dot{e}_h=U_2\sin(-k_2e_h)\end{cases}\tag{29}$$

Consider a Lyapunov function candidate

$$V_2(\boldsymbol{x})=\frac{1}{2}\left(e_v^2+e_h^2\right)\tag{34}$$

Derivative of $V_2(\boldsymbol{x})$ along the trajectories of system (29) can be taken as

$$\begin{aligned}\dot{V}_2(\boldsymbol{x}) &= \frac{\partial V_2(\boldsymbol{x})}{\partial \boldsymbol{x}} f(\boldsymbol{x}, G(\boldsymbol{x}), H(\boldsymbol{x}, G(\boldsymbol{x}))) \\ &= -e_v U_1 \sin(k_1 e_v) + e_h U_2 \sin(-k_2 e_h)\end{aligned} \tag{35}$$

Since $k_1 > 0, k_2 > 0, U_1 > 0$ and $U_2 > 0$, we compute $\dot{V}_2(\boldsymbol{x}) \leq 0$ and $\dot{V}_2(\boldsymbol{x}) < 0, \forall \boldsymbol{x} \neq 0$ in case of $|k_1 e_v| \leq \pi/2$ and $|k_2 e_h| \leq \pi/2$. Thereby, the asymptotic stability of system (29) near the equilibrium point is guaranteed.

To determine control laws $\overline{\tau}_q^{s2}$ and $\overline{\tau}_r^{s2}$, we resort to the degenerate equation $0 = g(\boldsymbol{x}, \boldsymbol{y}, H(\boldsymbol{x}, \boldsymbol{y}))$. It can be seen that the following control law will allow the control system to achieve the discussed goal.

$$\begin{cases} \overline{\tau}_q^{s2} = \left[k_3(k_1 e_v - \theta_e + \alpha) + q_p\right] d_{55} \\ \overline{\tau}_r^{s2} = \left[k_4(-k_2 e_h - \psi_e - \beta_n) + r_p\right] d_{66} \cos(\theta) \end{cases} \tag{36}$$

Here, $k_3 > 0$, $k_4 > 0$. Note that the choice of k_1 and k_2 determines how fast the tracking errors converge to zero.

4.2.2. Control law for the Layer-2 fast subsystem

Proposition 2. The *Layer-2* fast subsystem (26) will be asymptotically stable by selecting a simple control law

$$\begin{cases} \overline{\tau}_q^{f2} = -k_5 d_{55} \tilde{\theta}_e \\ \overline{\tau}_r^{f2} = -k_6 d_{66} \cos(\theta) \tilde{\psi}_e \end{cases} \tag{37}$$

where, $k_5 \geq 0$ and $k_6 \geq 0$.

Proof. Using (36) and (37), the *Layer-2* fast subsystem (26) is taken as

$$\begin{cases} \dfrac{d\tilde{\theta}_e}{dt_1} = \mu_1(-k_3 - k_5)\tilde{\theta}_e \\ \dfrac{d\tilde{\psi}_e}{dt_1} = \mu_1(-k_4 - k_6)\tilde{\psi}_e \end{cases} \tag{38}$$

Consider a Lyapunov function candidate

$$W_2(\boldsymbol{x}, \tilde{\boldsymbol{y}}) = \frac{1}{2}\left(\tilde{\theta}_e^2 + \tilde{\psi}_e^2\right) \tag{39}$$

We have

$$\begin{aligned}\dot{W}_2(\boldsymbol{x}, \tilde{\boldsymbol{y}}) &= \frac{\partial W_2(\boldsymbol{x}, \tilde{\boldsymbol{y}})}{\partial \tilde{\boldsymbol{y}}} \frac{1}{\mu_1} g(\boldsymbol{x}, \boldsymbol{y}, H(\boldsymbol{x}, \boldsymbol{y})) \\ &= -(k_3 + k_5)\tilde{\theta}_e^2 - (k_4 + k_6)\tilde{\psi}_e^2\end{aligned} \tag{40}$$

As $k_3 > 0$, $k_4 > 0$, $k_5 \geq 0$ and $k_6 \geq 0$, it is clear to see that $\dot{W}_2(\boldsymbol{x}, \tilde{\boldsymbol{y}}) \leq 0$ and $\dot{W}_2(\boldsymbol{x}, \tilde{\boldsymbol{y}}) < 0, \forall \tilde{\boldsymbol{y}} \neq 0$. Therefore, system (38) is asymptotically stable.

4.2.3. Control law for the Layer-1 fast subsystem

Similarly, the following proposition will guarantee the asymptotic stability of the *Layer-1* fast subsystem (24).

Proposition 3. The *Layer-1* fast subsystem (24) will be asymptotically stable by selecting

$$\begin{cases} \overline{\tau}_q^{f1} = -k_7\tilde{q} - k_8\tilde{w} \triangleq -k_7(q - \widehat{q}) - k_8(w - \widehat{w}) \\ \overline{\tau}_r^{f1} = -k_9\tilde{r} - k_{10}\tilde{v} \triangleq -k_9(r - \widehat{r}) - k_{10}(v - \widehat{v}) \end{cases} \tag{41}$$

where, $k_7 \geq 0$, $k_8 = m_{11}m_{55}u/m_{33}$, $k_9 \geq 0$ and $k_{10} = -m_{11}m_{66}u/m_{22}$. The quasi-steady-state $\widehat{v}$, $\widehat{w}$, $\widehat{q}$ and are expressed as

$$\widehat{v} = -\frac{m_{11}u}{d_{22}}\left[(k_6 + k_4)(-k_2 e_h - \psi_e - \beta_n) + r_p\right]\cos(\theta)$$

$$\widehat{w} = \frac{m_{11}u}{d_{33}}\left[(k_5 + k_3)(k_1 e_v - \theta_e + \alpha) + q_p\right]$$

$$\widehat{q} = (k_5 + k_3)(k_1 e_v - \theta_e + \alpha) + q_p$$

$$\widehat{r} = \left[(k_6 + k_4)(-k_2 e_h - \psi_e - \beta_n) + r_p\right]\cos(\theta)$$

Proof. Substituting (36), (37) and (41) into (24) yields the resultant *Layer-1* fast subsystem

$$\begin{cases} \dfrac{d\tilde{v}}{dt_2} = \mu_2 \dfrac{1}{m_{22}}(-m_{11}u\tilde{r} - d_{22}\tilde{v}) \\ \dfrac{d\tilde{w}}{dt_2} = \mu_2 \dfrac{1}{m_{33}}(m_{11}u\tilde{q} - d_{33}\tilde{w}) \\ \dfrac{d\tilde{q}}{dt_2} = \mu_2 \dfrac{1}{m_{55}}(-d_{55}\tilde{q} - k_7\tilde{q} - k_8\tilde{w}) \\ \dfrac{d\tilde{r}}{dt_2} = \mu_2 \dfrac{1}{m_{66}}(-d_{66}\tilde{r} - k_9\tilde{r} - k_{10}\tilde{v}) \end{cases} \tag{42}$$

Consider a Lyapunov function candidate

$$W_1(\boldsymbol{x}, \boldsymbol{y}, \tilde{\boldsymbol{z}}) = \frac{1}{2}\left(\tilde{v}^2 + \tilde{w}^2 + \tilde{q}^2 + \tilde{r}^2\right) \tag{43}$$

The derivative $\dot{W}_1(\boldsymbol{x}, \boldsymbol{y}, \tilde{\boldsymbol{z}})$ is given by

$$\begin{aligned}\dot{W}_1(\boldsymbol{x}, \boldsymbol{y}, \tilde{\boldsymbol{z}}) &= \frac{\partial W_1(\boldsymbol{x}, \boldsymbol{y}, \tilde{\boldsymbol{z}})}{\partial \tilde{\boldsymbol{z}}} \frac{1}{\mu_2} h(\boldsymbol{x}, \boldsymbol{y}, \boldsymbol{z}) \\ &= -\frac{1}{m_{22}}d_{22}\tilde{v}^2 - \frac{1}{m_{33}}d_{33}\tilde{w}^2 - \frac{1}{m_{55}}(d_{55} + k_7)\tilde{q}^2 \\ &\quad - \frac{1}{m_{66}}(d_{66} + k_9)\tilde{r}^2\end{aligned} \tag{44}$$

It is obvious that $\dot{W}_1(\boldsymbol{x}, \boldsymbol{y}, \tilde{\boldsymbol{z}}) \leq 0$ and $\dot{W}_1(\boldsymbol{x}, \boldsymbol{y}, \tilde{\boldsymbol{z}}) < 0, \forall \tilde{\boldsymbol{z}} \neq 0$, owing to $k_7 \geq 0$, $k_9 \geq 0$, $m_{22} > 0$, $m_{33} > 0$, $m_{55} > 0$, $m_{66} > 0$, $d_{22} > 0$, $d_{33} > 0$, $d_{55} > 0$ and $d_{66} > 0$. So, considering the control input as in (41), the origin of the *Layer-1* fast subsystem (24) is an asymptotically stable equilibrium point.

4.2.4. Overall control law

As illustration above, the feedback control law for system (14) is

$$\begin{cases} \tau_{q1} = -k_7\tilde{q} - k_8\tilde{w} + d_{55}\widehat{q} + mgz_g\sin(\theta) - (m_{33} - m_{11})uw \\ \tau_{r1} = -k_9\tilde{r} - k_{10}\tilde{v} + d_{66}\widehat{r} - (m_{11} - m_{22})uv \end{cases} \tag{45}$$

Recalling (11) and (12), the total feedback control law for system (10) is given at the same time. We observe that the proposed controller is a classical PID controller. This is an interesting connection between the proposed singular perturbation controller and the classical PID controller. On the basis of this observation, we come to a conclusion that the theory of singular perturbation and time scale may be a simple but effective method for PID control, since it provides a deep insight into the system properties and leads to a reduction of control complexity.

4.3. Stability analysis

In previous subsection, stability analysis of the reduced order subsystems has been provided. However, it guarantees only the

local stability of the equilibrium of the full dynamics (23). In this subsection, we will construct a composite Lyapunov function candidate for proving the asymptotic stability of dynamic model (23), meanwhile provide mathematical expressions for the upper bounds of those control gains.

In general, the derivative of α and β_n is vanishingly small, it is reasonable to suppose that $\dot{\alpha}=0$ and $\dot{\beta}_n=0$, which implies that α and β_n vary slowly relative to the other state variables. This assumption is quite natural for most small AUVs that move slowly in practical cases. On the basis of that, we rewrite system (23) as follow:

$$\begin{cases}\dot{\boldsymbol{x}}=f(\boldsymbol{x},G(\boldsymbol{x}),H(\boldsymbol{x},G(\boldsymbol{x})))+[f(\boldsymbol{x},\boldsymbol{y},H(\boldsymbol{x},\boldsymbol{y}))-f(\boldsymbol{x},G(\boldsymbol{x}),H(\boldsymbol{x},G(\boldsymbol{x})))]+\Delta F\\ \dot{\tilde{\boldsymbol{y}}}=\dfrac{1}{\varepsilon_1}g(\boldsymbol{x},\boldsymbol{y},H(\boldsymbol{x},\boldsymbol{y}))-\dfrac{\partial G(\boldsymbol{x})}{\partial \boldsymbol{x}}\dot{\boldsymbol{x}}+\Delta G\\ \dot{\tilde{\boldsymbol{z}}}=\dfrac{1}{\varepsilon_1\varepsilon_2}h(\boldsymbol{x},\boldsymbol{y},\boldsymbol{z})-\dfrac{\partial H(\boldsymbol{x},\boldsymbol{y})}{\partial(\boldsymbol{x},\boldsymbol{y})}\begin{bmatrix}\dot{\boldsymbol{x}}\\ \dot{\boldsymbol{y}}\end{bmatrix}\end{cases} \tag{46}$$

Here,

$$\Delta F=f(\boldsymbol{x},\boldsymbol{y},\tilde{\boldsymbol{z}}+H(\boldsymbol{x},\boldsymbol{y}))-f(\boldsymbol{x},\boldsymbol{y},H(\boldsymbol{x},\boldsymbol{y}))$$

$$\Delta G=\frac{1}{\varepsilon_1}[g(\boldsymbol{x},\boldsymbol{y},\tilde{\boldsymbol{z}}+H(\boldsymbol{x},\boldsymbol{y}))-g(\boldsymbol{x},\boldsymbol{y},H(\boldsymbol{x},\boldsymbol{y}))]$$

According to the strategy for time scale decomposition illustrated in section 4.1, we consider a composite Lyapunov function candidate

$$V(\boldsymbol{x},\tilde{\boldsymbol{y}},\tilde{\boldsymbol{z}})=(1-n_1)[(1-n_2)V_2(\boldsymbol{x})+n_2W_2(\boldsymbol{x},\tilde{\boldsymbol{y}})]+n_1W_1(\boldsymbol{x},\boldsymbol{y},\tilde{\boldsymbol{z}}) \tag{47}$$

Here, $0<n_{i=1,2}<1$.

Proposition 4. $V(\boldsymbol{x},\tilde{\boldsymbol{y}},\tilde{\boldsymbol{z}})$ is a Lyapunov function candidate for proving the asymptotic stability of the origin of singularly perturbed system (23), if the following conditions hold:

(1) $\frac{\partial V_2(\boldsymbol{x})}{\partial \boldsymbol{x}}f(\boldsymbol{x},G(\boldsymbol{x}),H(\boldsymbol{x},G(\boldsymbol{x})))\le-\alpha_{11}\varphi_{11}^2(x_1)-\alpha_{12}\varphi_{12}^2(x_2)$

(2) $\frac{\partial W_2(\boldsymbol{x},\tilde{\boldsymbol{y}})}{\partial \tilde{\boldsymbol{y}}}g(\boldsymbol{x},\boldsymbol{y},H(\boldsymbol{x},\boldsymbol{y}))\le-\alpha_{21}\varphi_{21}^2(\tilde{y}_1)-\alpha_{22}\varphi_{22}^2(\tilde{y}_2)$

(3) $\frac{\partial V_2(\boldsymbol{x})}{\partial \boldsymbol{x}}[f(\boldsymbol{x},\boldsymbol{y},H(\boldsymbol{x},\boldsymbol{y}))-f(\boldsymbol{x},G(\boldsymbol{x}),H(\boldsymbol{x},G(\boldsymbol{x})))]\le\beta_{11}\varphi_{11}(x_1)\varphi_{21}(\tilde{y}_1)+\beta_{21}\varphi_{12}(x_2)\varphi_{22}(\tilde{y}_2)$

(4) $\left[\frac{\partial W_2(\boldsymbol{x},\tilde{\boldsymbol{y}})}{\partial \boldsymbol{x}}-\frac{\partial W_2(\boldsymbol{x},\tilde{\boldsymbol{y}})}{\partial \tilde{\boldsymbol{y}}}\frac{\partial G(\boldsymbol{x})}{\partial \boldsymbol{x}}\right]f(\boldsymbol{x},\boldsymbol{y},H(\boldsymbol{x},\boldsymbol{y}))\le\beta_{12}\varphi_{11}(x_1)\varphi_{21}(\tilde{y}_1)+\beta_{13}\varphi_{21}^2(\tilde{y}_1)+\beta_{22}\varphi_{12}(x_2)\varphi_{22}(\tilde{y}_2)+\beta_{23}\varphi_{22}^2(\tilde{y}_2)$

(5) $\frac{\partial W_1(\boldsymbol{x},\boldsymbol{y},\tilde{\boldsymbol{z}})}{\partial \tilde{\boldsymbol{z}}}h(\boldsymbol{x},\boldsymbol{y},\boldsymbol{z})\le-a_{21}\vartheta_{21}^2(\tilde{z}_2,\tilde{z}_3)-a_{22}\vartheta_{22}^2(\tilde{z}_1,\tilde{z}_4)$

(6) $\frac{\partial[(1-n_2)V_2(\boldsymbol{x})+n_2W_2(\boldsymbol{x},\tilde{\boldsymbol{y}})]}{\partial(\boldsymbol{x},\tilde{\boldsymbol{y}})}\begin{bmatrix}\Delta F\\ \Delta G\end{bmatrix}\le b_{11}\vartheta_{11}(x_1,\tilde{y}_1)\vartheta_{21}(\tilde{z}_2,\tilde{z}_3)+b_{21}\vartheta_{12}(x_2,\tilde{y}_2)\vartheta_{22}(\tilde{z}_1,\tilde{z}_4)$

(7) $\left[\frac{\partial W_1(\boldsymbol{x},\boldsymbol{y},\tilde{\boldsymbol{z}})}{\partial(\boldsymbol{x},\boldsymbol{y})}-\frac{\partial W_1(\boldsymbol{x},\boldsymbol{y},\tilde{\boldsymbol{z}})}{\partial \tilde{\boldsymbol{z}}}\frac{\partial H(\boldsymbol{x},\boldsymbol{y})}{\partial(\boldsymbol{x},\boldsymbol{y})}\right]\begin{bmatrix}\dot{\boldsymbol{x}}\\ \dot{\boldsymbol{y}}\end{bmatrix}\le b_{12}\vartheta_{11}(x_1,\tilde{y}_1)\vartheta_{21}(\tilde{z}_2,\tilde{z}_3)+b_{13}\vartheta_{21}^2(\tilde{z}_2,\tilde{z}_3)+b_{22}\vartheta_{12}(x_2,\tilde{y}_2)\vartheta_{22}(\tilde{z}_1,\tilde{z}_4)+b_{23}\vartheta_{22}^2(\tilde{z}_1,\tilde{z}_4)$

Here, $x_{(\cdot)}$, $\tilde{y}_{(\cdot)}$ and $\tilde{z}_{(\cdot)}$ are the elements of vectors $\boldsymbol{x}$, $\tilde{\boldsymbol{y}}$ and $\tilde{\boldsymbol{z}}$, respectively. $\vartheta_{11}(x_1,\ \tilde{y}_1)=[\varphi_{11}(x_1);\varphi_{21}(\tilde{y}_1)]$, $\vartheta_{12}(x_2,\ \tilde{y}_2)=[\varphi_{12}(x_2);\varphi_{22}(\tilde{y}_2)]$. $\varphi_{ij}(\cdot)$ and $\vartheta_{ij}(\cdot)$ are continuous scalar positive-definite functions. $\alpha_{(\cdot)}$ and $a_{(\cdot)}$ are positive constants. $\beta_{(\cdot)}$ and $b_{(\cdot)}$ are nonnegative constants or matrices with nonnegative elements.

Proof. The derivation of these coefficients and functions is outlined in Appendix. The derivative $\dot{V}(\boldsymbol{x},\tilde{\boldsymbol{y}},\tilde{\boldsymbol{z}})$ is given by

$$\begin{aligned}\dot{V}(\boldsymbol{x},\tilde{\boldsymbol{y}},\tilde{\boldsymbol{z}})=&(1-n_1)(1-n_2)\frac{\partial V_2(\boldsymbol{x})}{\partial \boldsymbol{x}}f(\boldsymbol{x},G(\boldsymbol{x}),H(\boldsymbol{x},G(\boldsymbol{x})))+(1-n_1)\frac{n_2}{\varepsilon_1}\frac{\partial W_2(\boldsymbol{x},\tilde{\boldsymbol{y}})}{\partial \tilde{\boldsymbol{y}}}g(\boldsymbol{x},\boldsymbol{y},H(\boldsymbol{x},\boldsymbol{y}))\\&+(1-n_1)(1-n_2)\frac{\partial V_2(\boldsymbol{x})}{\partial \boldsymbol{x}}[f(\boldsymbol{x},\boldsymbol{y},H(\boldsymbol{x},\boldsymbol{y}))-f(\boldsymbol{x},G(\boldsymbol{x}),H(\boldsymbol{x},G(\boldsymbol{x})))]\\&+(1-n_1)n_2\left[\frac{\partial W_2(\boldsymbol{x},\tilde{\boldsymbol{y}})}{\partial \boldsymbol{x}}-\frac{\partial W_2(\boldsymbol{x},\tilde{\boldsymbol{y}})}{\partial \tilde{\boldsymbol{y}}}\frac{\partial G(\boldsymbol{x})}{\partial \boldsymbol{x}}\right]f(\boldsymbol{x},\boldsymbol{y},H(\boldsymbol{x},\boldsymbol{y}))+(1-n_1)\left\{\frac{\partial[(1-n_2)V_2(\boldsymbol{x})+n_2W_2(\boldsymbol{x},\tilde{\boldsymbol{y}})]}{\partial(\boldsymbol{x},\tilde{\boldsymbol{y}})}\begin{bmatrix}\Delta F\\ \Delta G\end{bmatrix}\right\}\\&+\frac{n_1}{\varepsilon_2\varepsilon_1}\frac{\partial W_1(\boldsymbol{x},\boldsymbol{y},\tilde{\boldsymbol{z}})}{\partial \tilde{\boldsymbol{z}}}h(\boldsymbol{x},\boldsymbol{y},\boldsymbol{z})+n_1\left\{\frac{\partial W_1(\boldsymbol{x},\boldsymbol{y},\tilde{\boldsymbol{z}})}{\partial(\boldsymbol{x},\boldsymbol{y})}-\frac{\partial W_1(\boldsymbol{x},\boldsymbol{y},\tilde{\boldsymbol{z}})}{\partial \tilde{\boldsymbol{z}}}\frac{\partial H(\boldsymbol{x},\boldsymbol{y})}{\partial(\boldsymbol{x},\boldsymbol{y})}\right\}\begin{bmatrix}\dot{\boldsymbol{x}}\\ \dot{\boldsymbol{y}}\end{bmatrix}\end{aligned} \tag{48}$$

Following that, substituting assumptions (1)–(7) into (48) yields an inequality

$$\begin{aligned}\dot{V}(\boldsymbol{x},\tilde{\mathbf{y}},\tilde{\mathbf{z}}) \le & -(1-n_1)(1-n_2)\left[\alpha_{11}\varphi_{11}^2(x_1)+\alpha_{12}\varphi_{12}^2(x_2)\right]-(1-n_1)\frac{n_2}{\varepsilon_1}\left[\alpha_{21}\varphi_{21}^2(\tilde{y}_1)+\alpha_{22}\varphi_{22}^2(\tilde{y}_2)\right]\\ & +(1-n_1)(1-n_2)[\beta_{11}\varphi_{11}(x_1)\varphi_{21}(\tilde{y}_1)+\beta_{21}\varphi_{12}(x_2)\varphi_{22}(\tilde{y}_2)]+(1-n_1)n_2\left[\beta_{12}\varphi_{11}(x_1)\varphi_{21}(\tilde{y}_1)+\beta_{13}\varphi_{21}^2(\tilde{y}_1)\right]\\ & +(1-n_1)n_2\left[\beta_{22}\varphi_{12}(x_2)\varphi_{22}(\tilde{y}_2)+\beta_{23}\varphi_{22}^2(\tilde{y}_2)\right]+(1-n_1)\{b_{11}\vartheta_{11}(x_1,\tilde{y}_1)\vartheta_{21}(\tilde{z}_2,\tilde{z}_3)+b_{21}\vartheta_{12}(x_2,\tilde{y}_2)\vartheta_{22}(\tilde{z}_1,\tilde{z}_4)\}\\ & -\frac{n_1}{\varepsilon_2\varepsilon_1}\left[a_{21}\vartheta_{21}^2(\tilde{z}_2,\tilde{z}_3)+a_{22}\vartheta_{22}^2(\tilde{z}_1,\tilde{z}_4)\right]+n_1\left[b_{12}\vartheta_{11}(x_1,\tilde{y}_1)\vartheta_{21}(\tilde{z}_2,\tilde{z}_3)+b_{13}\vartheta_{21}^2(\tilde{z}_2,\tilde{z}_3)\right]\\ & +n_1\left[b_{22}\vartheta_{12}(x_2,\tilde{y}_2)\vartheta_{22}(\tilde{z}_1,\tilde{z}_4)+b_{23}\vartheta_{22}^2(\tilde{z}_1,\tilde{z}_4)\right]\le -(1-n_1)\left[\vartheta_{11}^T(x_1,\tilde{y}_1)\Lambda_1\vartheta_{11}(x_1,\tilde{y}_1)+\vartheta_{12}^T(x_2,\tilde{y}_2)\Lambda_2\vartheta_{12}(x_2,\tilde{y}_2)\right]\\ & +(1-n_1)\{b_{11}\vartheta_{11}(x_1,\tilde{y}_1)\vartheta_{21}(\tilde{z}_2,\tilde{z}_3)+b_{21}\vartheta_{12}(x_2,\tilde{y}_2)\vartheta_{22}(\tilde{z}_1,\tilde{z}_4)\}-\frac{n_1}{\varepsilon_2\varepsilon_1}\left[a_{21}\vartheta_{21}^2(\tilde{z}_2,\tilde{z}_3)+a_{22}\vartheta_{22}^2(\tilde{z}_1,\tilde{z}_4)\right]\\ & +n_1\left[b_{12}\vartheta_{11}(x_1,\tilde{y}_1)\vartheta_{21}(\tilde{z}_2,\tilde{z}_3)+b_{13}\vartheta_{21}^2(\tilde{z}_2,\tilde{z}_3)\right]+n_1\left[b_{22}\vartheta_{12}(x_2,\tilde{y}_2)\vartheta_{22}(\tilde{z}_1,\tilde{z}_4)+b_{23}\vartheta_{22}^2(\tilde{z}_1,\tilde{z}_4)\right]\\ & \le -\Psi^T(x_1,\tilde{y}_1,\tilde{z}_2,\tilde{z}_3)\Pi_1\Psi(x_1,\tilde{y}_1,\tilde{z}_2,\tilde{z}_3)-\Gamma^T(x_2,\tilde{y}_2,\tilde{z}_1,\tilde{z}_4)\Pi_2\Gamma(x_2,\tilde{y}_2,\tilde{z}_1,\tilde{z}_4)\end{aligned} \tag{49}$$

where

$$\Psi(x_1,\tilde{y}_1,\tilde{z}_2,\tilde{z}_3)=\begin{bmatrix}\vartheta_{11}(x_1,\tilde{y}_1)\\ \vartheta_{21}(\tilde{z}_2,\tilde{z}_3)\end{bmatrix}\triangleq\begin{bmatrix}\varphi_{11}(x_1)\\ \varphi_{21}(\tilde{y}_1)\\ \vartheta_{21}(\tilde{z}_2,\tilde{z}_3)\end{bmatrix}$$

$$\Gamma(x_2,\tilde{y}_2,\tilde{z}_1,\tilde{z}_4)=\begin{bmatrix}\vartheta_{12}(x_1,\tilde{y}_1)\\ \vartheta_{22}(\tilde{z}_2,\tilde{z}_3)\end{bmatrix}\triangleq\begin{bmatrix}\varphi_{12}(x_2)\\ \varphi_{22}(\tilde{y}_2)\\ \vartheta_{22}(\tilde{z}_1,\tilde{z}_4)\end{bmatrix}$$

and

$$\Lambda_1=\begin{bmatrix}(1-n_2)\alpha_{11} & -0.5[(1-n_2)\beta_{11}+n_2\beta_{12}]\\ -0.5[(1-n_2)\beta_{11}+n_2\beta_{12}] & n_2\left(\frac{\alpha_{21}}{\varepsilon_1}-\beta_{13}\right)\end{bmatrix}$$

$$\Lambda_2=\begin{bmatrix}(1-n_2)\alpha_{12} & -0.5[(1-n_2)\beta_{21}+n_2\beta_{22}]\\ -0.5[(1-n_2)\beta_{21}+n_2\beta_{22}] & n_2\left(\frac{\alpha_{22}}{\varepsilon_1}-\beta_{23}\right)\end{bmatrix}$$

$$\Pi_1=\begin{bmatrix}(1-n_1)\Lambda_1 & -0.5[(1-n_1)b_{11}+n_1b_{12}]^T\\ -0.5[(1-n_1)b_{11}+n_1b_{12}] & n_1\left(\frac{a_{21}}{\varepsilon_1\varepsilon_2}-b_{13}\right)\end{bmatrix}$$

$$\Pi_2=\begin{bmatrix}(1-n_1)\Lambda_2 & -0.5[(1-n_1)b_{21}+n_1b_{22}]^T\\ -0.5[(1-n_1)b_{21}+n_1b_{22}] & n_1\left(\frac{a_{22}}{\varepsilon_1\varepsilon_2}-b_{23}\right)\end{bmatrix}$$

It is clear to see that the derivative of $V(\boldsymbol{x},\tilde{\boldsymbol{y}},\tilde{\boldsymbol{z}})$ along the trajectories of system (23) is negative definite, in case of Π_1 and Π_2 are both positive definite, namely, the following conditions hold:

$$|\Lambda_1|_d>0 \tag{50}$$

$$|\Lambda_2|_d>0 \tag{51}$$

$$|\Pi_1|_d>0 \tag{52}$$

$$|\Pi_2|_d>0 \tag{53}$$

Here, the operator $|\cdot|_d$ yields the determinant of a matrix. The detailed calculation is omitted for the sake of brevity.

Therefore, the origin of the three-time scale singularly perturbed system (23) is an asymptotically stable equilibrium point for control gains that satisfy the above conditions (50)–(53). In other word, the control gains are restricted in a certain region $D=\left\{k_{(\cdot)}\middle||\Lambda_{i=1,2}|_d>0,|\Pi_{i=1,2}|_d>0\right\}$.

5. Simulation results

In this section, the simulations results will be provided to illustrate the control performance of this closed-loop system, using an AUV model with physical and hydrodynamic characteristics as follows:

$m=185$, $d=0.02$, $m_{11}=215$, $m_{22}=265$, $m_{33}=265$, $m_{55}=80$, $m_{66}=80$, $Y_v=-300$, $Y_{v|v|}=-200$, $Z_w=-300$, $Z_{w|w|}=-200$, $M_q=-50$, $M_{q|q|}=-100$, $N_r=-50$ and $N_{r|r|}=-100$.

In order to demonstrate the robustness of the proposed controller, all these numerical simulations consider the systematical uncertainties and unknown disturbances given by

$$\begin{cases}d_q=1\times\text{rand}(1)+3\times\sin(0.01\times t)+1+0.2\times(d_{55}\times q)\\ d_r=1\times\text{rand}(1)+3\times\cos(0.01\times t)+1+0.2\times(d_{66}\times r)\end{cases}$$

Here, rand(1) is the zero-mean random noise with amplitude of 1.

The initial conditions of the vehicle is.

$[x(0),y(0),z(0)]=[0,20,0]$m, $[\phi(0),\theta(0),\psi(0)]=[0,0,0]$rad,

$[u(0),v(0),w(0)]=[1,0,0]$m/s, $[p(0),q(0),r(0)]=[0,0,0]$rad/s,

$\tau_q(0)=0$Nm, $\tau_r(0)=0$Nm.

In these simulations, the desired surge velocity is set to $u_d=1$m/s. The bounds for e_v, e_h, v, w, θ, α, $\dot{z}_p$, U_1 and U_2 are taken as $|e_v|\le 20$m, $|e_h|\le 30$m, $|v|\le 0.2$m/s, $|w|\le 0.2$m/s, $|\cos(\theta)|>0.5$, $|\cos(\theta-\alpha)|\ge 0.5$, $|\dot{z}_p|\le 0.5$, and thus $1\le U_1\le 1.12$, $0.5\le U_2\le 1.04$. To ensure the asymptotic stability of the closed-loop control system, the control gains for the proposed controller are selected as $\lambda_q=0.003$, $\lambda_r=0.003$, $k_1=0.075$, $k_2=0.04$, $k_3=0.4$, $k_4=0.4$, $k_5=0$, $k_6=0$, $k_7=500$, $k_8=m_{11}m_{55}u/m_{33}$, $k_9=600$ and $k_{10}=-m_{11}m_{66}u/m_{22}$.

Simulation results of following a cylindrical spiral desired path are provided in Figs. 5–8. Specifically, a simple observation of Fig. 5 (a) and (b) shows that, with the proposed controller, the underactuated AUV is capable of following the reference path even

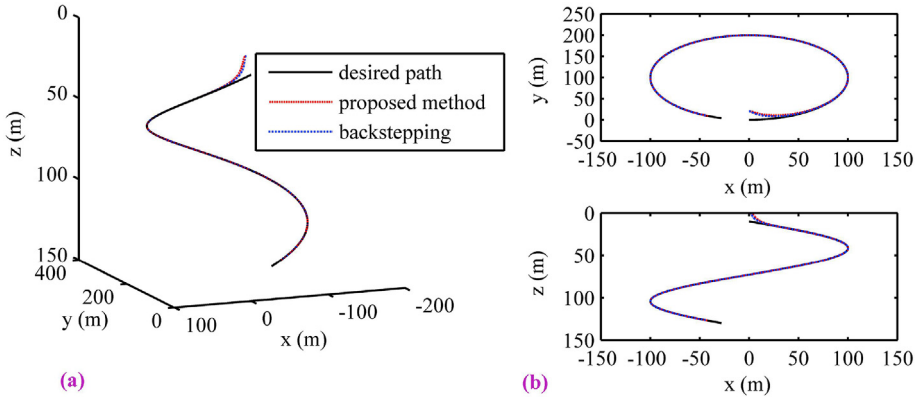

Fig. 5. Simulation results of following cylindrical spiral path. (a) 3D path; (b) paths projected on the horizontal and vertical planes.

though perturbed by internal and external disturbances. Fig. 6 illustrates that the tracking errors, sway and heave velocities, pitch and yaw rates converge to a small neighborhood of the origin. It can be seen that, during the transient, the response speed of the translational and angular velocities is faster than that of the tracking errors, at the same time, the response speed of the path angle tracking errors are faster than that of the cross-track errors. Therefore, the time scale decomposition mentioned-above is quite natural in some sense. Fig. 7 depicts the control inputs of the proposed method in pitch direction and in yaw direction. The given disturbances and the outputs of the ESO are plotted in Fig. 8. It reveals that the unknown disturbances, adding on the closed-loop control system, can be accurately estimated by the developed ESO, as noticed before.

Moreover, comparisons with the backstepping controller are provided. To this end, the simulation results, using the backstepping controller, are also plotted in Figs. 5–7. Referring to Figs. 5–7, one might find that the control performance of the

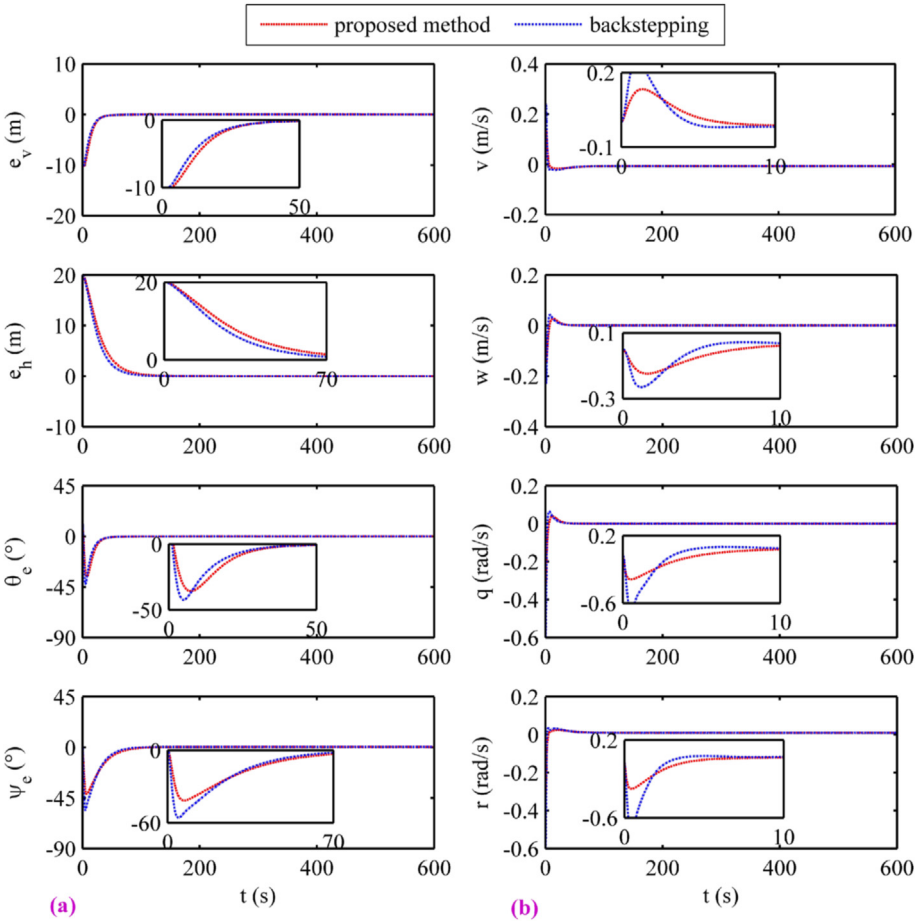

Fig. 6. Some important variables. (a) the tracking errors; (b) the translational and angular velocities.

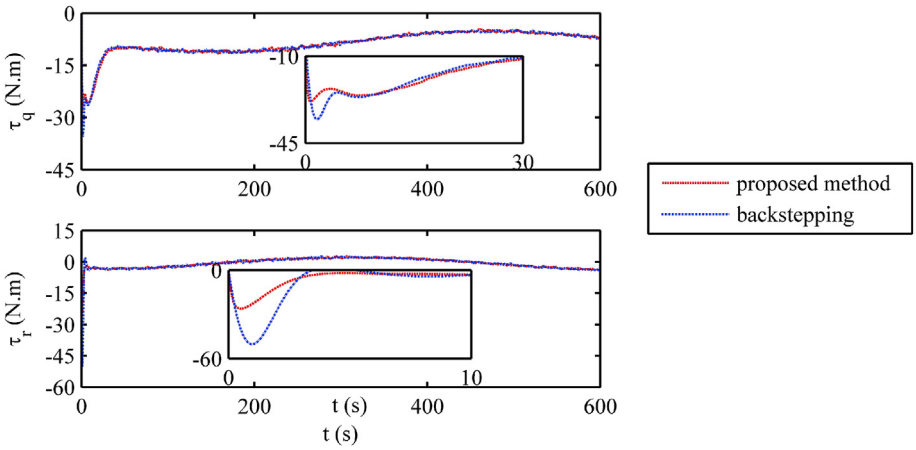

Fig. 7. Control inputs.

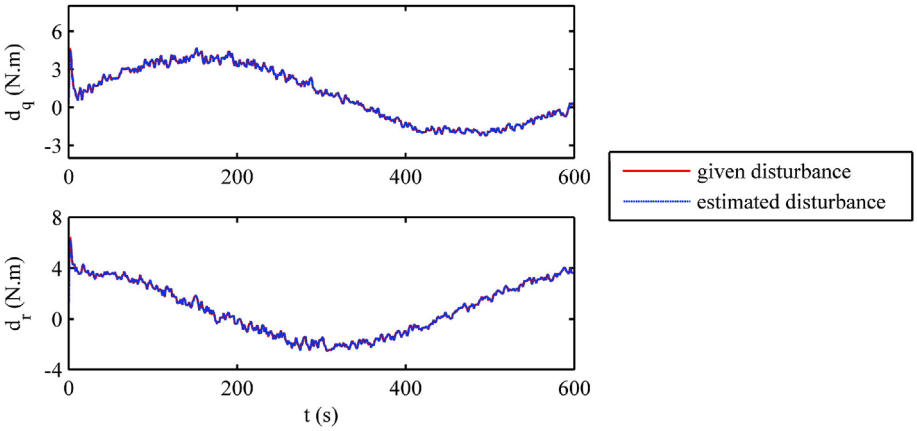

Fig. 8. Estimation performance by using the ESO.

singular perturbation controller is close to that of the backstepping controller, and the control inputs of the singular perturbation controller is smoother than that of the backstepping controller. Therefore, we come to a conclusion that the proposed controller is well behaved. And in implementations, the complexity of the proposed method is much simpler than that of the backstepping control, as noticed before. If considering the stability analysis, the complexity of these two methods will be similar.

In brief, the efficacy of the proposed approach to 3D path following control of underactuated AUVs subject to internal and external disturbances is therefore sufficiently demonstrated.

6. Conclusion

This paper considered the 3D path following control problem of underactuated AUVs subject to unknown internal and external disturbances. The overall path following controller was divided into two terms: an integrator and a stabilizing controller, using integral control method. By appropriately selecting the control gain, a time scale separation was artificially forced into the closed-loop control system. Singular perturbation theory was thus applied to analyze the system properties via order reduction. Specifically, the integrator was considered as a fast dynamical control law that designed to form a desired space configuration and, as a results, construct an ideal reduced model, in which the stabilizing controller was designed independently. To reduce the control complexity, the reduced model was decomposed into three subsystems by utilizing a forced singular perturbation method, followed by the design of each subsystem separately. Moreover, we proved the asymptotic stability of the closed-loop system with a composite Lyapunov function and provided mathematical bounds of the control gains. Simulation studies were also conducted to evaluate the control performance and a good path following ability was observed. They revealed that the proposed controller can stabilize the vehicle to desired path under unknown internal and external disturbances.

Declaration of competing interest

The authors declare that they have no known competing financial interests or personal relationships that could have appeared to influence the work reported in this paper.

Acknowledgments

This work is supported by the National Natural Science Foundation of China (Projects: 51879057, 51779052 and 51809064).

Appendix A

Proof of assumption (1)–(4).

Recalling (35) and (40), we satisfy conditions (1) and (2) with $\alpha_{11} = 2k_1u/\pi$, $\alpha_{11} = 2k_2|U_2|_{\min}/\pi$, $\alpha_{21} = \mu_1(k_3+k_5)$, $\alpha_{22} = \mu_1(k_4+k_6)$, $\varphi_{11}(x_1) = |e_v|$, $\varphi_{12}(x_2) = |e_h|$, $\varphi_{21}(\tilde{y}_1) = |\tilde{\theta}_e|$ and $\varphi_{22}(\tilde{y}_2) = |\tilde{\psi}_e|$. Using these results, we compute

$$\begin{aligned}
&\frac{\partial V_2(\boldsymbol{x})}{\partial \boldsymbol{x}}\left[f(\boldsymbol{x},\boldsymbol{y},H(\boldsymbol{x},\boldsymbol{y}))-f(\boldsymbol{x},G(\boldsymbol{x}),H(\boldsymbol{x},G(\boldsymbol{x})))\right]\\
&= e_v[-U_1\sin(\theta_e-\alpha)+U_1\sin(\widehat{\theta}_e-\alpha)]+e_h[U_2\sin(\psi_e+\beta_n)\\
&\quad -U_2\sin(\widehat{\psi}_e+\beta_n)]\\
&\le |U_1|_{max}\varphi_{11}(x_1)\varphi_{21}(\tilde{y}_1)+|U_2|_{max}\varphi_{12}(x_2)\varphi_{22}(\tilde{y}_2)
\end{aligned}$$

and

$$\begin{aligned}
&\left[\frac{\partial W_2(\boldsymbol{x},\tilde{\boldsymbol{y}})}{\partial \boldsymbol{x}}-\frac{\partial W_2(\boldsymbol{x},\tilde{\boldsymbol{y}})}{\partial \tilde{\boldsymbol{y}}}\frac{\partial G(\boldsymbol{x})}{\partial \boldsymbol{x}}\right]f(\boldsymbol{x},\boldsymbol{y},H(\boldsymbol{x},\boldsymbol{y}))\\
&= k_1\tilde{\theta}_eU_1\sin(\theta_e-\alpha)-k_2\tilde{\psi}_eU_2\sin(\psi_e+\beta_n)\\
&\le k_1|\tilde{\theta}_e||U_1|_{max}(|\tilde{\theta}_e|+k_1|e_v|)+k_2|\tilde{\psi}_e||U_2|_{max}(\tilde{\psi}_e+k_2|e_h|)\\
&\le k_1|U_1|_{max}(k_1\varphi_{11}(x_1)+\varphi_{21}(\tilde{y}_1))\varphi_{21}(\tilde{y}_1)\\
&\quad +k_2|U_2|_{max}(k_2\varphi_{12}(x_2)+\varphi_{22}(\tilde{y}_2))\varphi_{22}(\tilde{y}_2)
\end{aligned}$$

thereby satisfy assumptions (3) and (4) with $\beta_{11} = |U_1|_{\max}$, $\beta_{21} = |U_2|_{\max}$, $\beta_{12} = {k_1}^2|U_1|_{\max}$, $\beta_{13} = k_1|U_1|_{\max}$, $\beta_{22} = {k_2}^2|U_2|_{\max}$ and $\beta_{23} = k_2|U_2|_{\max}$.

Proof of assumption (5)–(7).

Recalling (44), we satisfy the assumption (5) with $a_{21} = a_{22} = \mu_2$, $\vartheta_{21}(\tilde{z}_2,\tilde{z}_3) = \left[|d_{33}|_{min}\tilde{w}^2/m_{33}+(|d_{55}|_{min}+k_7)\tilde{q}^2/m_{55}\right]^{1/2}$ and $\vartheta_{22}(\tilde{z}_1,\tilde{z}_4) = \left[|d_{22}|_{min}\tilde{v}^2/m_{22}+(|d_{66}|_{min}+k_9)\tilde{r}^2/m_{66}\right]^{1/2}$. Following that,

$$\begin{aligned}
&\frac{\partial[(1-n_2)V_2(\boldsymbol{x})+n_2W_2(\boldsymbol{x},\tilde{\boldsymbol{y}})]}{\partial(\boldsymbol{x},\tilde{\boldsymbol{y}})}\begin{bmatrix}\Delta F\\ \Delta G\end{bmatrix}=n_2\tilde{\theta}_e\tilde{q}+n_2\tilde{\psi}_e\frac{1}{\cos(\theta)}\tilde{r}\\
&\le \frac{n_2}{\sqrt{(|d_{55}|_{min}+k_7)/m_{55}}}\varphi_{21}(\tilde{y}_1)\vartheta_{21}(\tilde{z}_2,\tilde{z}_3)\\
&\quad +\frac{n_2}{|\cos(\theta)|_{min}}\frac{1}{\sqrt{(|d_{66}|_{min}+k_9)/m_{66}}}\varphi_{22}(\tilde{y}_2)\vartheta_{22}(\tilde{z}_1,\tilde{z}_4)
\end{aligned}$$

and

$$\begin{aligned}
&\left[\frac{\partial W_1(\boldsymbol{x},\boldsymbol{y},\tilde{\boldsymbol{z}})}{\partial(\boldsymbol{x},\boldsymbol{y})}-\frac{\partial W_1(\boldsymbol{x},\boldsymbol{y},\tilde{\boldsymbol{z}})}{\partial\tilde{\boldsymbol{z}}}\frac{\partial H(\boldsymbol{x},\boldsymbol{y})}{\partial(\boldsymbol{x},\boldsymbol{y})}\right]\begin{bmatrix}\dot{\boldsymbol{x}}\\ \dot{\boldsymbol{y}}\end{bmatrix}\\
&= k_1(k_5+k_3)\left(\frac{m_{11}u}{d_{33}}\tilde{w}+\tilde{q}\right)U_1\sin(\theta_e-\alpha)-k_2(k_6+k_4)cos(\theta)\\
&\quad\times\left(\frac{m_{11}u}{d_{22}}\tilde{v}-\tilde{r}\right)U_2\sin(\psi_e+\beta_n)+(k_5+k_3)\left(\frac{m_{11}u}{d_{33}}\tilde{w}+\tilde{q}\right)\left(q\right.\\
&\quad\left.-q_p\right)-(k_6+k_4)\cos(\theta)\left(\frac{m_{11}u}{d_{22}}\tilde{v}-\tilde{r}\right)\left(\frac{1}{\cos(\theta)}r-r_p\right)\\
&\le (k_5+k_3)Ak_1^2|U_1|_{max}\varphi_{11}(x_1)\vartheta_{21}(\tilde{z}_2,\tilde{z}_3)+(k_5\\
&\quad +k_3)A[k_1|U_1|_{max}+(k_5+k_3)]\varphi_{21}(\tilde{y}_1)\vartheta_{21}(\tilde{z}_2,\tilde{z}_3)+(k_5\\
&\quad +k_3)A\frac{1}{\sqrt{(|d_{55}|_{min}+k_7)/m_{55}}}\vartheta_{21}^2(\tilde{z}_2,\tilde{z}_3)+(k_6\\
&\quad +k_4)Bk_2^2|U_2|_{max}\varphi_{12}(x_2)\vartheta_{22}(\tilde{z}_1,\tilde{z}_4)+(k_6+k_4)B[k_2|U_2|_{max}\\
&\quad +(k_6+k_4)]\varphi_{22}(\tilde{y}_2)\vartheta_{22}(\tilde{z}_1,\tilde{z}_4)+(k_6\\
&\quad +k_4)B\frac{1}{\sqrt{(|d_{66}|_{min}+k_9)/m_{66}}}\vartheta_{22}^2(\tilde{z}_1,\tilde{z}_4)
\end{aligned}$$

Here,

$$A=\frac{m_{11}u}{|d_{33}|_{\min}}\frac{1}{\sqrt{|d_{33}|_{\min}/m_{33}}}+\frac{1}{\sqrt{(|d_{55}|_{\min}+k_7)/m_{55}}}$$

$$B=\frac{m_{11}u}{|d_{22}|_{\min}}\frac{1}{\sqrt{|d_{22}|_{\min}/m_{22}}}+\frac{1}{\sqrt{(|d_{66}|_{\min}+k_9)/m_{66}}}$$

Therefore, we satisfy the assumptions (6) and (7) with

$$b_{11}=\begin{bmatrix}0\\ n_2\frac{1}{\sqrt{(|d_{55}|_{\min}+k_7)/m_{55}}}\end{bmatrix}$$

$$b_{21}=\begin{bmatrix}0\\ n_2\frac{1}{|\cos(\theta)|_{\min}}\frac{1}{\sqrt{(|d_{66}|_{\min}+k_9)/m_{66}}}\end{bmatrix}$$

$$b_{12}=(k_5+k_3)A\begin{bmatrix}{k_1}^2|U_1|_{max}\\ k_1|U_1|_{max}+(k_5+k_3)\end{bmatrix}$$

$$b_{22}=(k_6+k_4)B\begin{bmatrix}{k_2}^2|U_2|_{max}\\ k_2|U_2|_{max}+(k_6+k_4)\end{bmatrix}$$

$$b_{13}=(k_5+k_3)A\frac{1}{\sqrt{(|d_{55}|_{\min}+k_7)/m_{55}}}$$

$$b_{23}=(k_6+k_4)B\frac{1}{\sqrt{(|d_{66}|_{\min}+k_9)/m_{66}}}$$

References

Aguiar, A.P., Hespanha, J.P., 2007. Trajectory-tracking and path-following of underactuated autonomous vehicles with parametric modeling uncertainty. IEEE Trans. Automat. Contr. 52 (8), 1362–1379.

Bhatta, P., Leonard, N.E., 2008. Nonlinear gliding stability and control for vehicles with hydrodynamic forcing. Automatica 44 (5), 1240–1250.

Canudas, d.W.C., Olguin, D.O., 2000. Nonlinear control of an underwater vehicle/manipulator with composite dynamics. IEEE Trans. Contr. Syst. Technol. 8 (6), 948–960.

Do, K., Pan, J., Jiang, Z., 2004. Robust and adaptive path following for underactuated autonomous underwater vehicles. Ocean. Eng. 31 (16), 1967–1997.

Elmokadem, T., Zribi, M., Youcef-Toumi, K., 2016. Trajectory tracking sliding mode control of underactuated AUVs. Nonlinear Dynam. 84 (2), 1079–1091.

Fernandes, D., Sorensen, A.J., Pettersen, K.Y., Donha, D.C., 2015. Output feedback motion control system for observation class ROVs based on a high-gain state observer: theoretical and experimental results. Contr. Eng. Pract. 39, 90–102.

Joe, H., Kim, M., Yu, S.C., 2014. Second-order sliding mode controller for autonomous underwater vehicle in the presence of unknown disturbances. Nonlinear Dynam. 78 (1), 183–196.

Khalil, H.K., 2002. Nonlinear Systems, third ed. Prentice Hall, Upper Saddle River.

Kokotovic, P., Khalil, H.K., O'reilly, J., 1999. Singular Perturbation Methods in Control: Analysis and Design. ACADEMIC PRESS INC.

Lapierre, L., Jouvencel, B., 2008. Robust nonlinear path-following control of an AUV. IEEE J. Ocean. Eng. 33 (2), 89–102.

Lei, M., 2020. Nonlinear diving stability and control for an AUV via singular perturbation. Ocean. Eng. 197.

Lekkas, A.M., Fossen, T.I., 2013. Line-of-Sight guidance for path following of marine vehicles (Chapter 5). Book: Advanced in Marine Robotics. Lambert Academic Publishing.

Park, B.S., 2015. Adaptive formation control of underactuated autonomous underwater vehicles. Ocean. Eng. 96, 1–7.

Peng, Z.H., Wang, J., 2018b. Output-feedback path following control of autonomous underwater vehicles based on an extended state observer and projection neural networks. IEEE Transactions on Systems, Man, and Cybernetics: Systems 48 (4), 535–544.

Peng, Z., Wang, J., Han, Q.L., 2018. Path-following control of autonomous underwater vehicles subject to velocity and input constraints via neurodynamic optimization. IEEE Trans. Ind. Electron. 66 (11), 8724–8732.

Peng, Z.H., Wang, J.S., Wang, J., 2019. Constrained control of autonomous underwater vehicles based on command optimization and disturbance estimation. IEEE Trans. Ind. Electron. 66 (5), 3627–3635.

Peymani, E., Fossen, T.I., 2015. Path following of underwater robots using Lagrange multipliers. Robot. Autonom. Syst. 67, 44–52.

Prestero, T., 2001. Verification of a Six-Degree of Freedom Simulation Model for the REMUS Autonomous Underwater Vehicle. Ph.D. Thesis, Massachusetts Institute of Technology.

Qi, X., 2014. Adaptive coordinated tracking control of multiple autonomous underwater vehicles. Ocean. Eng. 91, 84–90.

Ren, R.Y., Zou, Z.J., Wang, X.G., 2014. A two-time scale control law based on singular perturbations used in rudder roll stabilization of ships. Ocean. Eng. 88, 488–498.

Rezazadegan, F., Shojaei, K., Sheikholeslam, F., Chatraei, A., 2015. A novel approach to 6-dof adaptive trajectory tracking control of an AUV in the presence of parameter uncertainties. Ocean. Eng. 107, 246–258.

Saberi, A., Khalil, H.K., 1984. Quadratic-type Lyapunov functions for singularly perturbed systems. IEEE Trans. Automat. Contr. 29, 542–550.

Salgado-Jimenez, T., Spiewak, J.M., Fraisse, P., Jouvencel, B., 2004. A robust control algorithm for AUV: based on a high order sliding mode. Proceedings of the MTS/IEEE International Conference. OCEANS'04, Kobe, Japan, pp. 276–281.

Sheu, D., Vinh, N.X., Howe, R.M., 1991. Application of singular perturbation methods for three-dimensional minimum-time interception. J. Guid. Contr. Dynam. 14 (2), 360–367.

Shinar, J., 1983. On applications of singular perturbation techniques in nonlinear optimal control. Automatica 19 (2), 203–211.

Xiang, X., Yu, C., Zhang, Q., 2017. Robust fuzzy 3D path following for autonomous underwater vehicle subject to uncertainties. Comput. Oper. Res. 84, 165–177.

Xu, J., Wang, M., Qiao, L., 2015. Dynamical sliding mode control for the trajectory tracking of underactuated unmanned underwater vehicles. Ocean. Eng. 105, 54–63.

Yi, B.W., Qiao, L., Zhang, W.D., 2016. Two-time scale path following of underactuated marine surface vessels: design and stability analysis using singular perturbation methods. Ocean. Eng. 124, 287–297.

Zhang, F., Tan, X., 2015. Passivity-based stabilization of underwater gliders with a control surface. J. Dyn. Syst. Meas. Contr. 137 (6), 061006.

Zhang, L.J., Qi, X., Pang, Y.J., 2009. Adaptive output feedback control based on DRFNN for AUV. Ocean. Eng. 36, 716–722.